

A Reduced Three Dimensional Dynamic Structural Model for Structural Health Assessment

Luther White
Department of Mathematics
University of Oklahoma
Norman, Oklahoma 73019
lwhite@ou.edu

April 19, 2006

Abstract

Dynamic models of elastic structures are derived using approximations of linear three dimensional elasticity. A model for the three dimensional motion of a nonsymmetric structure that is of use for applications to health monitoring for buildings is obtained. The symmetric version of the model is validated using laboratory acceleration data. Narrow plate equations whose derivation is based on similar consideration but with plate thinness assumptions are used in a probabilistic inversion for elastic and mass properties from acceleration data. Finally, predictions of structural behavior based on the information from the inversion problem are made.

1. Introduction.

We derive three dimensional dynamic models for structures. The derivation is analogous to that of the so-called narrow plate models of intermediate natural between beams and plates. In [7, 8, 9] narrow plate models are presented. Also, narrow plate models are validated against spectral data and static models are studied. In the current work, however, dynamic time dependent models are presented and derived without the thickness assumption imposed on plates [2,4,7,8,9]. Displacement approximations are assumed that are similar to those for narrow plates and generalizations of Timoshenko beam models [1]. However, they are specializations of the Mindlin plate model [4]. The objective of our modelling effort is to obtain a three dimensional model that is suitable for assessment of the structural health of buildings. Our model allows for nonsymmetric properties in the structure. However, at this early stage of development we present the model, but compare only to laboratory structures that are sym-

metric. A numerical inversion of acceleration data is presented as well as predictions of likely structural responses based on a posteriori probability density functions.

In Section 2 we present the derivation of the equations that include base motion. The derivations are based on the small displacement gradient assumption of linear elasticity [2]. Geometric symmetry of the structure about a central axis is assumed. However, in order to accommodate possible structural damage, material properties are not assumed symmetric. The spatially discrete time dependent model is presented that includes a moving base. In Section 3 we present a specialization of our model to the classical Euler-Bernoulli beam with a tip mass to illustrate a comparison between our model and the tip mass model. In Section 4 we compare our computed accelerations with those observed in the laboratory. We find that our results qualitatively support this application of the model. In Section 5 we formulate an inverse problem using acceleration data to provide probabilistic estimates of material parameters. These estimates are then used to make predictions of likely behavior of the structure under a given force.

2. The underlying model equations.

Although the sets for which we develop our theory are more general than the rectangular solid we deal with here, we focus here on sets Ω in \mathbf{R}^3 defined by

$$\Omega = \{(x, y, z) : 0 < x < L, -k < y < k, -h < z < h\}.$$

The parameters k and h are assumed to be roughly the same size. Displacements in the x , y , and z directions are designated by u , v , and w , respectively, as indicated in Figure 1.

We assume the material is isotropic and the small displacement gradient assumption applies [2]. The strains are expressed as

$$(2.1) \quad \begin{aligned} \epsilon_{11} &= \frac{\partial u}{\partial x} \\ \epsilon_{12} &= \frac{1}{2} \left(\frac{\partial u}{\partial y} + \frac{\partial v}{\partial x} \right) \\ \epsilon_{13} &= \frac{1}{2} \left(\frac{\partial u}{\partial z} + \frac{\partial w}{\partial x} \right) \\ \epsilon_{22} &= \frac{\partial v}{\partial y} \\ \epsilon_{23} &= \frac{1}{2} \left(\frac{\partial v}{\partial z} + \frac{\partial w}{\partial y} \right) \end{aligned}$$

$$\epsilon_{33} = \frac{\partial w}{\partial z}.$$

The stresses are expressed as

$$(2.2) \quad \begin{aligned} \sigma_{11} &= \frac{E}{(1+\mu)(1-2\mu)} [(1-\mu)\epsilon_{11} + \mu\epsilon_{22} + \mu\epsilon_{33}] \\ \sigma_{12} &= \frac{2E}{1+\mu} \epsilon_{12} \\ \sigma_{13} &= \frac{2E}{1+\mu} \epsilon_{13} \\ \sigma_{22} &= \frac{E}{(1+\mu)(1-2\mu)} [\mu\epsilon_{11} + (1-\mu)\epsilon_{22} + \mu\epsilon_{33}] \\ \sigma_{23} &= \frac{2E}{1+\mu} \epsilon_{23} \\ \sigma_{33} &= \frac{E}{(1+\mu)(1-2\mu)} [\mu\epsilon_{11} + \mu\epsilon_{22} + (1-\mu)\epsilon_{33}] \end{aligned}$$

where E is Young's modulus and μ is Poisson's ratio. We do not impose geometric assumptions on the stresses at this point as is done with beam and plate models. Nevertheless, displacements are constrained under an assumption that the length dimensions in the y and z dimensions are roughly the same order. The displacement functions are expanded as truncated series in y and z with coefficients as functions of x . Towards this end displacement functions

$$(2.3) \quad \begin{aligned} u(x, y, z) &= u_0(x) + zu_1(x) + yu_2(x) + yzu_3(x) \\ v(x, y, z) &= v_0(x) + zv_1(x) + z^2v_2(x) \\ w(x, y, z) &= w_0(x) + yw_1(x) + y^2w_2(x). \end{aligned}$$

These expressions amount to approximation in the y and z variables in a physically meaningful way. The stress-free boundary conditions on the lateral faces are variational boundary conditions and, hence, are not imposed on the approximating elements. It follows that the corresponding strains are given by

$$(2.4) \quad \begin{aligned} \epsilon_{11} &= u_{0x} + zu_{1x} + yu_{2x} + yzu_{3x} \\ \epsilon_{12} &= \frac{1}{2} \{u_2 + v_{0x} + z(u_3 + v_{1x}) + z^2v_{2x}\} \\ \epsilon_{13} &= \frac{1}{2} \{u_1 + w_{0x} + y(u_3 + w_{2x}) + y^2w_{2x}\} \end{aligned}$$

$$\epsilon_{22} = 0$$

$$\epsilon_{23} = \frac{1}{2}\{v_1 + w_1 + 2zv_2 + 2yw_2\}$$

$$\epsilon_{33} = 0.$$

The stresses are expressed as

$$(2.5) \quad \begin{aligned} \sigma_{11} &= \frac{(1-\mu)E}{(1+\mu)(1-2\mu)}[u_{0x} + zu_{1x} + yu_{2x} + yzu_{3x}] \\ \sigma_{12} &= \frac{2E}{1+\mu}[u_2 + v_{0x} + z(u_3 + v_{1x}) + z^2v_{2x}] \\ \sigma_{13} &= \frac{2E}{1+\mu}[u_1 + w_{0x} + y(u_3 + w_{1x}) + y^2w_{2x}] \\ \sigma_{22} &= \frac{\mu E}{(1+\mu)(1-2\mu)}[u_{0x} + zu_{1x} + yu_{2x} + yzu_{3x}] \\ \sigma_{23} &= \frac{2E}{1+\mu}[v_1 + w_1 + 2zv_2 + 2yw_2] \\ \sigma_{33} &= \frac{\mu E}{(1+\mu)(1-2\mu)}[u_{0x} + zu_{1x} + yu_{2x} + yzu_{3x}]. \end{aligned}$$

The energy due to strain is expressed as

$$(2.6) \quad \begin{aligned} V &= \frac{1}{2} \int_{\Omega} \{ \sigma_{11}\epsilon_{11} + 2\sigma_{12}\epsilon_{12} + \\ &\quad + 2\sigma_{13}\epsilon_{13} + \sigma_{22}\epsilon_{22} + 2\sigma_{23}\epsilon_{23} + \sigma_{33}\epsilon_{33} \} dz dy dx \end{aligned}$$

Substituting relations from (2.4) and (2.5) into (2.6), we obtain

$$(2.7) \quad \begin{aligned} V &= \frac{1}{2} \int_{\Omega} \left\{ \frac{(1-\mu)E}{(1+\mu)(1-2\mu)} [u_{0x} + zu_{1x} + yu_{2x} + yzu_{3x}]^2 \right. \\ &\quad + \frac{2E}{1+\mu} [u_2 + v_{0x} + z(u_3 + v_{1x}) + z^2v_{2x}]^2 + \\ &\quad + \frac{2E}{1+\mu} [u_1 + w_{0x} + y(u_3 + w_{1x}) + y^2w_{2x}]^2 + \\ &\quad \left. + \frac{2E}{1+\mu} [v_1 + w_1 + 2zv_2 + 2yw_2]^2 \right\} dz dy dx. \end{aligned}$$

The Young's modulus E and Poisson's ratio μ are taken to be dependent on the spatial variables. In general no symmetry in the functions E and μ is assumed; hence,

$$E = E(x, y, z)$$

and

$$\mu = \mu(x, y, z).$$

Define the following matrix-valued functions of x .

(2.8)

$$k_0(x) = \int_{-k}^k \int_{-h}^h \frac{(1 - \mu(x, y, z))E(x, y, z)}{(1 + \mu(x, y, z))(1 - 2\mu(x, y, z))} \begin{bmatrix} 1 & z & y & yz \\ z & z^2 & yz & yz^2 \\ y & yz & y^2 & y^2z \\ yz & yz^2 & y^2z & y^2z^2 \end{bmatrix} dzdy$$

(2.9)

$$a_0(x) = \int_{-k}^k \int_{-h}^h \frac{2E(x, y, z)}{1 + \mu(x, y, z)} \begin{bmatrix} 1 & z & z^2 \\ z & z^2 & z^3 \\ z^2 & z^3 & z^4 \end{bmatrix} dzdy$$

(2.10)

$$b_0(x) = \int_{-k}^k \int_{-h}^h \frac{2E(x, y, z)}{1 + \mu(x, y, z)} \begin{bmatrix} 1 & y & y^2 \\ y & y^2 & y^3 \\ y^2 & y^3 & y^4 \end{bmatrix} dzdy$$

(2.11)

$$c_0(x) = \int_{-k}^k \int_{-h}^h \frac{2E(x, y, z)}{1 + \mu(x, y, z)} \begin{bmatrix} 1 & 2z & 2y \\ 2z & 4z^2 & 4zy \\ 2y & 4zy & 4y^2 \end{bmatrix} dzdy.$$

With these assignments the strain potential energy takes the form

$$(2.12) \quad V = \frac{1}{2} \int_0^L \{ [u_0 \ u_1 \ u_2 \ u_3]_x k_0(x) \begin{bmatrix} u_0 \\ u_1 \\ u_2 \\ u_3 \end{bmatrix}_x + [u_2 + v_{0x} \ u_3 + v_{1x} \ v_{2x}] a_0(x) \begin{bmatrix} u_2 + v_{0x} \\ u_3 + v_{1x} \\ v_{2x} \end{bmatrix} + [u_1 + w_{0x} \ u_3 + w_{1x} \ w_{2x}] b_0(x) \begin{bmatrix} u_1 + w_{0x} \\ u_3 + w_{1x} \\ w_{2x} \end{bmatrix} + [v_1 + w_1 \ v_2 \ w_2] c_0(x) \begin{bmatrix} v_1 + w_1 \\ v_2 \\ w_2 \end{bmatrix} \} dx.$$

Define the vector-valued function $x \mapsto \mathbf{V}(x)$ from $\mathbf{R} \mapsto \mathbf{R}^{10}$

$$\mathbf{V}(x) = [u_0(x) \ u_1(x) \ u_2(x) \ u_3(x) \ v_0(x) \ v_1(x) \ v_2(x) \ w_0(x) \ w_1(x) \ w_2(x)]^T$$

where T designates vector transpose. We write the strain energy explicitly in terms of \mathbf{V} by introducing the following matrices

$$\begin{aligned} P_u &= \begin{bmatrix} 1 & 0 & 0 & 0 & 0 & 0 & 0 & 0 & 0 & 0 \\ 0 & 1 & 0 & 0 & 0 & 0 & 0 & 0 & 0 & 0 \\ 0 & 0 & 1 & 0 & 0 & 0 & 0 & 0 & 0 & 0 \\ 0 & 0 & 0 & 1 & 0 & 0 & 0 & 0 & 0 & 0 \end{bmatrix} \\ P_v &= \begin{bmatrix} 0 & 0 & 0 & 0 & 1 & 0 & 0 & 0 & 0 & 0 \\ 0 & 0 & 0 & 0 & 0 & 1 & 0 & 0 & 0 & 0 \\ 0 & 0 & 0 & 0 & 0 & 0 & 1 & 0 & 0 & 0 \end{bmatrix} \\ P_w &= \begin{bmatrix} 0 & 0 & 0 & 0 & 0 & 0 & 0 & 1 & 0 & 0 \\ 0 & 0 & 0 & 0 & 0 & 0 & 0 & 0 & 1 & 0 \\ 0 & 0 & 0 & 0 & 0 & 0 & 0 & 0 & 0 & 1 \end{bmatrix} \\ P_1 &= \begin{bmatrix} 0 & 1 & 0 & 0 & 0 & 0 & 0 & 0 & 0 & 0 \\ 0 & 0 & 0 & 1 & 0 & 0 & 0 & 0 & 0 & 0 \\ 0 & 0 & 0 & 0 & 0 & 0 & 0 & 0 & 0 & 0 \end{bmatrix} \\ P_2 &= \begin{bmatrix} 0 & 0 & 1 & 0 & 0 & 0 & 0 & 0 & 0 & 0 \\ 0 & 0 & 0 & 1 & 0 & 0 & 0 & 0 & 0 & 0 \\ 0 & 0 & 0 & 0 & 0 & 0 & 0 & 0 & 0 & 0 \end{bmatrix} \\ P_3 &= \begin{bmatrix} 0 & 0 & 0 & 0 & 0 & 1 & 0 & 0 & 1 & 0 \\ 0 & 0 & 0 & 0 & 0 & 0 & 1 & 0 & 0 & 0 \\ 0 & 0 & 0 & 0 & 0 & 0 & 0 & 0 & 0 & 1 \end{bmatrix}. \end{aligned}$$

With these assignments, the strain energy functional may be written as

$$(2.13) \quad V = \frac{1}{2} \int_0^L \{ \mathbf{V}_x^T P_u^T k_0(x) P_u \mathbf{V}_x + [P_2 \mathbf{V} + P_v \mathbf{V}_x]^T a_0(x) [P_2 \mathbf{V} + P_v \mathbf{V}_x] + \\ + [P_1 \mathbf{V} + P_w \mathbf{V}_x]^T b_0(x) [P_1 \mathbf{V} + P_w \mathbf{V}_x] + \mathbf{V}^T P_3^T c_0(x) P_3 \mathbf{V} \} dx.$$

Finally, for convenience define the matrices

$$(2.14) \quad \mathbf{k}(x) = P_u^T k_0(x) P_u + P_v^T a_0(x) P_v + P_w^T b_0(x) P_w$$

$$(2.14) \quad \mathbf{a}(x) = P_2^T a_0(x) P_2 + P_w^T b_0(x) P_1$$

$$(2.15) \quad \mathbf{b}(x) = P_2^T a_0(x) P_2 + P_1^T b_0(x) P_1 + P_3^T c_0(x) P_3$$

and express the strain energy as

$$(2.16) \quad V = \frac{1}{2} \int_0^L \{ \mathbf{V}_x^T \mathbf{k}(x) \mathbf{V}_x + \mathbf{V}_x^T \mathbf{a}(x) \mathbf{V} + \mathbf{V}^T \mathbf{a}(x)^T \mathbf{V}_x + \mathbf{V}^T \mathbf{b}(x) \mathbf{V} \} dx.$$

To introduce dynamics, we assume that the functions u, v , and w are dependent also on time t so that $\mathbf{V} = \mathbf{V}(x, t)$. Introducing the density function $(x, y, z) \mapsto \rho(x, y, z)$ defined on Ω , the kinetic energy quadratic functional is given as

$$(2.17) \quad K = \frac{1}{2} \int_{\Omega} \rho(x, y, z) [u_t^2 + v_t^2 + w_t^2] dz dy dx$$

where the displacement functions are considered to be dependent on time as well as space. Substituting the expressions from (2.3) for u, v , and w , we have

$$(2.18) \quad K = \frac{1}{2} \int_{\Omega} \rho(x, y, z) \{ [u_{0t} + zu_{1t} + yu_{2t} + yzu_{3t}]^2 + [v_{0t} + zv_{1t} + z^2v_{2t}]^2 + [w_{0t} + zw_{1t} + z^2w_{2t}]^2 \} dz dy dx.$$

Introducing the matrix

$$(2.19) \quad \mathbf{m}(x) = \int_{-k}^k \int_{-h}^h \rho(x, y, z) \begin{bmatrix} 1 & z & y & yz & 0 & 0 & 0 & 0 & 0 & 0 \\ z & z^2 & yz & yz^2 & 0 & 0 & 0 & 0 & 0 & 0 \\ y & yz & y^2 & y^2z & 0 & 0 & 0 & 0 & 0 & 0 \\ yz & yz^2 & y^2z & y^2z^2 & 0 & 0 & 0 & 0 & 0 & 0 \\ 0 & 0 & 0 & 0 & 1 & z & z^2 & 0 & 0 & 0 \\ 0 & 0 & 0 & 0 & z & z^2 & z^3 & 0 & 0 & 0 \\ 0 & 0 & 0 & 0 & z^2 & z^3 & z^4 & 0 & 0 & 0 \\ 0 & 0 & 0 & 0 & 0 & 0 & 0 & 1 & y & y^2 \\ 0 & 0 & 0 & 0 & 0 & 0 & 0 & y & y^2 & y^3 \\ 0 & 0 & 0 & 0 & 0 & 0 & 0 & y^2 & y^3 & y^4 \end{bmatrix} dz dy,$$

the expression for kinetic energy can be written as

$$(2.20) \quad T = \frac{1}{2} \int_0^L \mathbf{V}_t(x, t)^T \mathbf{m}(x) \mathbf{V}_t(x, t) dx.$$

The work done by external forces is expressed as

$$(2.21) \quad W = \int_0^L \mathbf{f}(x, t)^T \mathbf{V}(x, t) dx.$$

Forming the Lagrangian and applying Hamilton's principle [5] yields an initial boundary value problem. Finally, including a damping term for energy dissipation, we obtain

$$(2.22) \quad \mathbf{m}\mathbf{V}_{tt} + \mathbf{c}\mathbf{V}_t - (\mathbf{k}\mathbf{V}_x + \mathbf{a}\mathbf{V})_x + \mathbf{a}^T\mathbf{V}_x + \mathbf{b}\mathbf{V} = \mathbf{f}$$

with initial conditions

$$(2.23) \quad \mathbf{V}(\cdot, 0) = \mathbf{V}_0$$

$$\mathbf{V}(\cdot, 0) = \mathbf{V}_1$$

and boundary conditions that must satisfy

$$\delta\mathbf{V}(\mathbf{k}\mathbf{V}_x + \mathbf{a}\mathbf{V})|_0^L = \mathbf{0}.$$

Under boundary conditions that are clamped at $x = 0$ and free at $x = L$, we have

$$(2.24) \quad \mathbf{V}(0, t) = \mathbf{0}$$

and

$$(2.25) \quad (k\mathbf{V}_x + \mathbf{a}\mathbf{V})(L, t) = \mathbf{0}.$$

For many applications we want to include the possibility of a moving base. Thus, we wish to have a boundary condition

$$\mathbf{V}(0, t) = \mathbf{W}(t)$$

To adjust our model, we define a new function

$$(2.26) \quad \mathbf{U}(x, t) = \mathbf{V}(x, t) - \mathbf{W}(t)$$

and substitute into the differential equation. Carrying out this procedure, we obtain the equation

$$(2.27) \quad \begin{aligned} \mathbf{m}\mathbf{U}_{tt} + \mathbf{c}\mathbf{U}_t - (\mathbf{k}\mathbf{U}_x + \mathbf{a}\mathbf{U})_x + \mathbf{a}^T\mathbf{U}_x + \mathbf{b}\mathbf{U} &= \\ &= \mathbf{f} - [\mathbf{m}\mathbf{W}_{tt} + \mathbf{c}\mathbf{W}_t - (\mathbf{a}\mathbf{W})_x + \mathbf{b}\mathbf{W}] \end{aligned}$$

with boundary conditions

$$(2.28) \quad \mathbf{U}(0, t) = \mathbf{0}$$

$$(2.29) \quad [\mathbf{k}\mathbf{U}_x + \mathbf{a}\mathbf{U}](L, t) = -\mathbf{a}\mathbf{W}(t).$$

Semidiscrete spatial approximations may be obtained using piecewise linear elements defined on a nonuniform mesh on $(0, L)$, [6]. Let the interval $(0, L)$ be

partitioned into N subintervals $[x_i, x_{i+1}]$ and let $M = N + 1$. Let $\{b_i$ for $i = 1, \dots, M\}$ be the functions given by

$$b_i(x) = \begin{cases} \frac{x-x_{i-2}}{x_{i-1}-x_{i-2}} & \text{for } x \in [x_{i-2}, x_{i-1}], \\ \frac{x_i-x}{x_i-x_{i-1}} & \text{for } x \in [x_{i-1}, x_i], \\ 0 & \text{otherwise,} \end{cases}$$

Define the column M vector-valued function $x \mapsto \mathbf{b}(x) = [b_1(x), \dots, b_M(x)]^T$, and let $\mathbf{0}$ designate an M row-vector of zeros. Finally, define the $10 \times 10M$ matrix valued function

$$x \mapsto B(x) = \begin{bmatrix} \mathbf{b}(x)^T & \mathbf{0} & \dots & \mathbf{0} & \mathbf{0} \\ \mathbf{0} & \mathbf{b}(x)^T & \mathbf{0} & \dots & \mathbf{0} \\ \dots & \dots & \dots & \dots & \dots \\ \mathbf{0} & \mathbf{0} & \dots & \mathbf{0} & \mathbf{b}(x)^T \end{bmatrix}$$

Let $t \mapsto \mathbf{c}(t)$ denote the mapping from \mathbf{R} into \mathbf{R}^{10M} where $\mathbf{c}(t)$ is a column vector for each value of t . We consider functions to approximate the solution \mathbf{U} of the above initial boundary value problem expressed in the form

$$\mathbf{U}^N(x, t) = B(x)\mathbf{c}(t).$$

Define the $10M \times 10M$ matrices

$$(2.30) \quad M = \int_0^L B(x)^T \mathbf{m}(x) B(x) dx$$

$$(2.31) \quad C = \int_0^L B(x)^T \mathbf{c}(x) B(x) dx$$

$$(2.32) \quad K = \int_0^L [B_x^T(x) \mathbf{k}(x) B_x(x) + B_x^T(x) \mathbf{a}(x) B(x) + B^T(x) \mathbf{a}^T(x) B_x(x) + B^T(x) \mathbf{b}(x) B(x)] dx$$

and the column vector

$$\mathbf{F} = \int_0^L B(x)^T [f - (\mathbf{m}W_{tt} + \mathbf{c}W_t + \mathbf{b}W)] dx.$$

We use the weak form of the boundary value problem to obtain

$$(2.33) \quad M\mathbf{c}_{tt} + C\mathbf{c}_t + K\mathbf{c} = \mathbf{F}$$

with initial conditions

$$(2.34) \quad \mathbf{c}(0) = \mathbf{0}$$

$$(2.35) \quad \mathbf{c}_t(0) = \mathbf{0}.$$

3. Comparison of model with simple Euler-Bernoulli with tip-mass.

In this section we specialize the model derived in Section 2 to show its relation to the classic Euler-Bernoulli beam with a tip-mass. We assume the beam is symmetric about the x axis and the beam density is piecewise constant on $(0, L)$ and constant for $x \in (0, L_1)$ and $x \in (L_1, L)$, respectively, see Figure 2. Our equation for the beam with a tip mass is obtained as L_1 is allowed to approach L . To obtain the Euler-Bernoulli beam equation consider the displacement relations

$$(3.1) \quad \begin{aligned} u(x, y, z) &= -zw_{0x}(x) \\ v(x, y, z) &= 0 \\ w(x, y, z) &= w_0(x) \end{aligned}$$

in which the displacement in the x direction is due solely to the transverse bending. In this case the strains are given as

$$(3.2) \quad \begin{aligned} \epsilon_{11} &= -zw_{0xx} \\ \epsilon_{12} = \epsilon_{13} = \epsilon_{22} = \epsilon_{23} = \epsilon_{33} &= 0. \end{aligned}$$

The stresses are expressed as

$$(3.3) \quad \begin{aligned} \sigma_{11} &= -\frac{z(1-\mu)E}{(1+\mu)(1-2\mu)}w_{0xx} \\ \sigma_{12} = \sigma_{13} = \sigma_{22} = \sigma_{23} = \sigma_{33} &= 0. \end{aligned}$$

It follows that the strain energy is given by

$$(3.4) \quad V = \frac{1}{2} \int_{\Omega} \left\{ \frac{(1-\mu)E}{(1+\mu)(1-2\mu)} [zw_{0xx}]^2 dz dy dx \right.$$

Integrating with respect to y and z , we obtain

$$(3.5) \quad V = \frac{1}{2} \int_0^L \frac{4h^3k(1-\mu)E}{3(1+\mu)(1-2\mu)} w_{0xx}^2 dx$$

The the expression for kinetic energy is determined as

$$(3.6) \quad K = \frac{1}{2} \int_0^L \rho(x) \left\{ \frac{4h^3k}{3} w_{0xt}^2 + 4hkw_{0t}^2 \right\} dx.$$

Under the assumption that h is small, the h^3 term is neglected. Hence, the kinetic energy is

$$(3.7) \quad K = \frac{1}{2} \int_0^L \rho(x) 4hk w_{0t}^2 dx.$$

Since the density ρ is piecewise constant, we write

$$(3.8) \quad K = \frac{1}{2} \left\{ \int_0^{L_1} \frac{m_1}{4hkL_1} 4hk w_{0t}^2 dx + \int_{L_1}^L \frac{m}{4hk(L-L_1)} 4hk w_{0t}^2 dx \right\}.$$

To obtain the tip mass expression, we take the limit of (3.8) as $L_1 \rightarrow L$. Assuming the continuity of w_{0t} we obtain the result

$$(3.9) \quad K = \frac{1}{2} \int_0^L \rho w_{0t}^2 dx + \frac{m}{2} w_0(L, t)_t^2$$

where ρ represents a linear density $\rho = \frac{m}{L}$. The Lagrangian is thus given by

$$\mathcal{L} = \frac{1}{2} \int_0^{t_f} \{K - V\} dt$$

and

$$(3.10) \quad \mathcal{L} = \frac{1}{2} \int_0^{t_f} \left\{ m w_{0t}^2(L, t) + \int_0^L \left[\rho w_{0t}^2 + \frac{4h^3 k (1-\mu) E}{3(1+\mu)(1-2\mu)} w_{0xx}^2 \right] dx \right\} dt$$

Calculating the variation of \mathcal{L} , we obtain from Hamilton's principle [5] that

$$(3.11) \quad \begin{aligned} \rho w_{0tt} &= \frac{4h^3(1-\mu)E}{3(1+\mu)(1-2\mu)} w_{0xxxx} \text{ in } (0, L) \times (0, t_f) \\ w_0(0, t) &= w_{0x}(0, t) = 0 \text{ for } t \in (0, t_f) \\ w_{0xx}(L, t) &= 0 \text{ for } t \in (0, t_f) \\ w_{0tt}(L, t) &= -\frac{4h^3(1-\mu)E}{3(1+\mu)(1-2\mu)} w_{0xxx}(L, t) \text{ for } t \in (0, t_f) \end{aligned}$$

The expressions (3.10) and (3.11) coincide with those obtained for the Euler-Bernoulli beam with tip mass [1]. Results comparing tip motion of a beam with tip mass for the Euler-Bernoulli model and the narrow plate model described in the previous section are compared in Figure 3. Certainly, the narrow plate model has some higher frequency content. However, the correlation between the two output is high at 0.94.

4. The comparison of model output with laboratory data.

We assume that the Young's modulus, Poisson's ratio, and density are functions of x only

$$E = E(x), \quad \mu = \mu(x), \quad \text{and} \quad \rho = \rho(x)$$

the matrices k_0 , a_0 , b_0 , and m are expressed as

$$k_0(x) = \frac{(1 - \mu(x))E(x)}{(1 + \mu(x))(1 - 2\mu(x))} \begin{bmatrix} 4hk & 0 & 0 & 0 \\ 0 & \frac{4h^3k}{3} & 0 & 0 \\ 0 & 0 & \frac{4hk^3}{3} & 0 \\ 0 & 0 & 0 & \frac{4h^3k^3}{9} \end{bmatrix}$$

$$a_0(x) = \frac{2E(x)}{1 + \mu(x)} \begin{bmatrix} 4hk & 0 & \frac{4h^3k}{3} \\ 0 & \frac{4h^3k}{3} & 0 \\ \frac{4h^3k}{3} & 0 & \frac{4h^5k}{5} \end{bmatrix}$$

$$b_0(x) = \frac{2E(x)}{1 + \mu(x)} \begin{bmatrix} 4hk & 0 & \frac{4hk^3}{3} \\ 0 & \frac{4hk^3}{3} & 0 \\ \frac{4hk^3}{3} & 0 & \frac{4hk^5}{5} \end{bmatrix}$$

$$c_0(x) = \frac{2E(x)}{1 + \mu(x)} \begin{bmatrix} 4hk & 0 & 0 \\ 0 & \frac{16h^3k}{3} & 0 \\ 0 & 0 & \frac{16hk^3}{3} \end{bmatrix}.$$

$$\mathbf{m}(x) = \rho(x) \begin{bmatrix} 4hk & 0 & 0 & 0 & 0 & 0 & 0 & 0 & 0 & 0 \\ 0 & \frac{4h^3k}{3} & 0 & 0 & 0 & 0 & 0 & 0 & 0 & 0 \\ 0 & 0 & \frac{4hk^3}{3} & 0 & 0 & 0 & 0 & 0 & 0 & 0 \\ 0 & 0 & 0 & \frac{4h^3k^3}{9} & 0 & 0 & 0 & 0 & 0 & 0 \\ 0 & 0 & 0 & 0 & 4hk & 0 & \frac{4h^3k}{3} & 0 & 0 & 0 \\ 0 & 0 & 0 & 0 & 0 & \frac{4h^3k}{3} & 0 & 0 & 0 & 0 \\ 0 & 0 & 0 & 0 & \frac{4h^3k}{3} & 0 & \frac{4h^5k}{5} & 0 & 0 & 0 \\ 0 & 0 & 0 & 0 & 0 & 0 & 0 & 4hk & 0 & \frac{4hk^3}{3} \\ 0 & 0 & 0 & 0 & 0 & 0 & 0 & 0 & \frac{4hk^3}{3} & 0 \\ 0 & 0 & 0 & 0 & 0 & 0 & 0 & \frac{4hk^3}{3} & 0 & \frac{4hk^5}{5} \end{bmatrix}.$$

The structure is depicted in Figure 4. The length of the structure is 31 inches with the base 1 inch, floor 1 from 10 to 11 inches, floor 2 from 20 to 21 inches, and floor 3 from 30 to 31 inches. The mass of the structure is concentrated in the base and floors 1,2, and 3. The structure is disturbed by shaking the base. The resulting acceleration time series of length 16000 with measurements at every 0.01 seconds is recorded along with observed accelerations at floors 1, 2, and 3.

We thus set the force vector \mathbf{f} to zero and obtain the associated base velocity and displacement vector functions by integrating the acceleration record. In fact we use a Daubechy level 12 wavelet approximation to smooth the acceleration time series [3]. Base motion is portrayed in Figure 5. To approximate the equation, we use a finite element basis of piecewise linear functions described previously based on nodal locations

$$[0 \ 1 \ 4 \ 7 \ 10 \ 11 \ 14 \ 17 \ 20 \ 21 \ 24 \ 27 \ 30 \ 31].$$

At this point we are interested primarily in the qualitative behavior of our model. Hence, we set $\mu = 0$. The only modelling of Young's modulus and density is that values of these parameters in intervals corresponding to the floors is very large as compared with those intervals associated with regions between floors. A small constant viscous damping term is also included. The initial value problem is solved numerically using a 1 sec time step and compared with the Daubechy 12 wavelet approximation of the observed acceleration time series over a time period of 155 seconds. The results are portrayed in Figures 6, 7, and 8. We note that there is high correlation between signals over subintervals of the record in which initial effects are not included. For the second floor a comparison of a shifted records results in very high correlation of 0.97 compared to the 0.71 correlation without shifting. For these examples this seems to be qualitative evidence of a valid model.

5. Inversion of acceleration data.

In this section we use acceleration data to estimate material properties of a structure. We consider a slightly different set of displacement relations.

$$\begin{aligned} u(x, y, z, t) &= u_0(x, t) + zu_1(x, t) + yzu_2(x, t) \\ v(x, y, z, t) &= v_0(x, t) + zv_1(x, t) + yzv_2(x, t) \\ w(x, y, z, t) &= w_0(x, t) + yw_1(x, t) + y^2w_2(x, t). \end{aligned}$$

The model that we consider, a narrow "bowed" plate, that is derived with the above displacement relations and makes the plate thickness assumption that normal forces on the surface may be view as body forces. The stress σ_{33} is set to zero, and the resulting relation is used to solve for ϵ_{33} it terms of ϵ_{11} and ϵ_{22} , see [7,8,9]. A system of initial boundary value problems analogous to those obtained in Section 2 are obtained by means of a similar procedure. In this case we have a system of nine partial differential equations with a single spatial variable. The solution is a column 9-vector $V(x, t) = [u_0, u_1, u_2, v_0, v_1, v_2, w_0, w_1, w_2](x, t)^T$. The model we study allows for a base that satisfies a time dependent boundary condition. In this particular instance, we consider a base motion defined by

$$V(0, t) = Amp * \nu(t)$$

where

$$Amp = \begin{bmatrix} 0 & 0 & 0 & 0 & 0 & 0 & 0 & 0 & 0 \\ 0 & 0 & 0 & 0 & 0 & 0 & 0 & 0 & 0 \\ 0 & 0 & 0 & 0 & 0 & 0 & 0 & 0 & 0 \\ 0 & 0 & 0 & 0 & 0 & 0 & 0 & 0 & 0 \\ 0 & 0 & 0 & 0 & 0 & 0 & 0 & 0 & 0 \\ 0 & 0 & 0 & 0 & 0 & 0 & 0 & 0 & 0 \\ 0 & 0 & 0 & 0 & 0 & 0 & 1 & 0 & 0 \\ 0 & 0 & 0 & 0 & 0 & 0 & 0 & 0.25 & 0 \\ 0 & 0 & 0 & 0 & 0 & 0 & 0 & 0 & 0 \end{bmatrix}$$

and

$$t \mapsto \nu(t)$$

is a vector valued function whose entries are

$$\nu_i(t) = \begin{cases} \sin(\pi t/30) & \text{for } 0 \leq t \leq 30 \\ 0 & \text{otherwise,} \end{cases}$$

for $i = 1, \dots, 9$. In this application the boundary conditions are imposed by penalization to force the structure boundary to comply with the specified boundary condition. Figure 9 depicts a deformation in which t is less than 30 while Figure 10 shows a deformation in which t is greater than 30. In [7,8,9] estimation problems are considered from an optimization point of view to determine parameters from among an admissible set minimizing the L^2 norm of the error between simulated output and observed output. Here we take a probabilistic point of view and introduce a pdf constructed using the error that is defined on a sample space consisting of admissible parameters, cf. [10]. The resulting joint pdf carries the information from the model and the data on the parameters. Initially the parameters are considered independent. Correlations among them are a consequence of the model mapping taking parameters to system output.

The motivating application is the structure in Figure 4. However, in this case we view the elastic, density, and damping parameters to be constants with floors 1, 2, and 3 modelled as point masses at $L/3$, $2L/3$, and L . In this model even though the thickness assumptions apparently do not hold, torsional and bowing motions of the structure are allowed. We define a parameter vector

$$q = [m_1, m_2, m_3, \mu, E, \rho, d_0]^T,$$

and we consider the mapping

$$q \mapsto V(q)(x, t) \mapsto z(q)(t) = [w_{tt}(L/3, t), w_{tt}(2L/3, t), w_{tt}(L, t)]^T$$

that associates a parameter q with an output that is the transverse acceleration at the points $L/3$, $2L/3$, and L .

To test an inversion technique numerically, it is common to study an "identical twin problem" in which a parameter q_0 is specified and the associated output

$z_0(t) = V(q_0)(t) + \text{noise}$ is calculated. This output is then used in the inversion algorithm to recover the parameter q_0 , or to determine the information supplied by the data. This is done by defining a fit-to-data criterion

$$J(q) = \int_0^{t_f} (z(q)(t) - z_0(t))^T M(z(q)(t) - z_0(t)) dt$$

expressing the error between computed outputs and the data. A "solution" of the estimation problem is a minimizer of $J(q)$ over the admissible parameter set Q .

In stochastic or probabilistic inversion, a probability density function over the set Q by

$$q \mapsto f(q) = C \exp\left[-\frac{1}{2}J(q)\right].$$

The constant C is introduced as a normalization factor so that

$$\int_Q f(q) dq = 1.$$

This resulting joint pdf contains information on the parameters from the admissible set that is embodied in the data $z_0(t)$. It may be used to gain information on individual or combinations of the parameters through marginalization. We may also determine the information gained by comparing probability intervals calculated from the pdf obtained from the data with those determined without data. This comparison enables us to assess the added value of the data over our a priori information. In addition, using the joint pdf, we can make predictions on the probable behavior of the structure based on available information. The structure's behavior may be viewed as a random variable defined on the sample space Q . Thus, we may compute the distribution for that random variable resulting from the data.

A drawback of the "identical twin" approach is that many times a given method may work well with some q_0 , but not with others. Our approach is to view the parameters q_0 themselves as random variables and consider an ensemble of problems. If no problem is any more likely than any other, then the generating parameters q_0 may be considered to be uniformly distributed over the admissible set Q . On the other hand, if there is information indicating some problems are more likely than others, then this may be reflected in the choice of the example problems. Here we view the q_0 as uniformly distributed over Q and consider an ensemble of problems chosen randomly over Q using a uniformly distributed random number generator. We present ratios of 0.95 probability between a posteriori marginal distributions determined with the benefit of data and marginal distributions obtained without the benefit of additional data. These are then averaged over the ensemble of problems to obtain an indicator of how much information on a particular parameter is obtained from the data.

The admissible set of parameters is the set Q that is specified using the following bounds on parameters.

Minimum and maximum parameter bounds

| parameter | minimum | maximum |
|-----------------|---------|---------|
| mass1 | 0.5 | 2.5 |
| mass2 | 0.5 | 2.5 |
| mass3 | 0.5 | 2.5 |
| Poisson's ratio | 0 | 0.5 |
| Young's modulus | 1 | 20.0 |
| density | 0.25 | 0.75 |
| damping | 0.0 | 0.02 |

The results of the ensemble identical twin examples are given in the following table. The last column indicates the ratio of the 0.95 probability interval divided by 0.95 times the length of the intervals in the previous table. This is an indicator of the reduction of the 0.95 interval due to the data and gives an idea as to the general value of the data in estimating the parameter.

0.95 Probability intervals and ratios

| parameter | 0.025 | 0.975 | difference | difference for uniform distribution | ratio |
|-----------------|-------|-------|------------|-------------------------------------|-------|
| mass1 | 0.086 | 1.75 | 1.66 | 1.9 | 0.87 |
| mass2 | 0.091 | 1.66 | 1.57 | 1.9 | 0.82 |
| mass3 | 0.14 | 1.73 | 1.59 | 1.9 | 0.83 |
| Poisson's ratio | 0.034 | 0.44 | 0.41 | 0.47 | 0.86 |
| Young's modulus | 4.16 | 16.7 | 1.25 | 18.1 | 0.69 |
| density | 0.286 | 0.695 | 0.409 | 0.47 | 0.86 |
| damping | 0.002 | 0.018 | 0.016 | 0.019 | 0.85 |

From this table we observe that in all cases the 0.95 probability interval as been reduced with the inclusion of the data. Apparently the Young's modulus has benefited most with at reduction of 31 percent.

While the marginal distributions give information of the individual parameters, a further indicator as to the value of the data is its impact on prediction of state properties. Our view is that the joint pdf contains the information of the material properties of the structure. We then can use the joint pdf to predict the likely response of the structure under other conditions. For example, we considered the prediction of the kinetic energy of mass 3 in a case in which there is an activating point force on the structure at $x = L/2$. Thus, we view the kinetic energy for as a random variable depending on the parameters

$q \in Q$. As such, the cumulative distribution of the kinetic energy may be calculated. In Figure 11 is presented the cumulative distributions obtained in the presence of data and without the benefit of the data. That is, the a priori pdf as simply the uniform distribution over Q and the a posteriori pdf with data are used to calculate the distribution of the kinetic energy. The steeper curve is the cdf obtained with data and indicates that there is a probability of 0.95 that the kinetic energy is between 0.015 and 0.03. Without the data there is a 0.95 probability that the kinetic energy is between 0.01 and 0.12. For this case the data has brought about a substantial narrowing of the 0.95 interval for the predicted response of the structure and thereby has substantially increased our information on the state of the system.

References

- [1] Graff, K.F., *Wave Motion in Elastic Solids*, Ohio State University Press, Columbus, Ohio, 1975.
- [2] Hunter, S.C., *Mechanics of Continuous Media*, Ellis Horwood, New York, 1976.
- [3] *Matlab Wavelet Toolbox User's Guide*, The Math Works, Inc., 1996.
- [4] Mindlin, R.D., *Influence of rotatory inertia and shear on flexural motions of isotropic elastic plates*, Journal of Applied Mechanics, March, 1951, pp 31-38.
- [5] Meirovitch, L., *Analytic Methods in Vibrations*, MacMillan, London, 1967.
- [6] Schultz, M. *Spline Analysis*, Prentice-Hall, Englewood Cliffs, NJ, 1973.
- [7] Russell, D. and L. White, *Identification of Parameters in Narrow Plate Models from Spectral Data*, Journal of Mathematical Analysis and Applications, 197, (1996), pp 679-707.
- [8] Russell, D. and L. White, *Formulation and Validation of Dynamical Models for Narrow Plate Motion*, Journal Applied Mathematics and Computation, 58, (1993), pp 103-141.
- [9] Russell, D. and L. White, *The Bowed Narrow Plate Model*, Electronic Journal of Differential Equations, April(2000).
- [10] Tarantola, A., *Inverse Problem Theory*, Elsevier, New York, 1987.

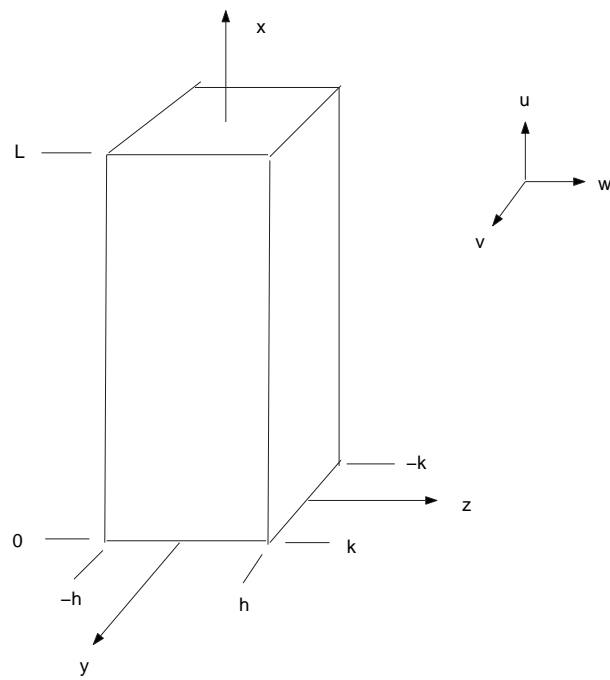


Figure 1: Formulation of the model

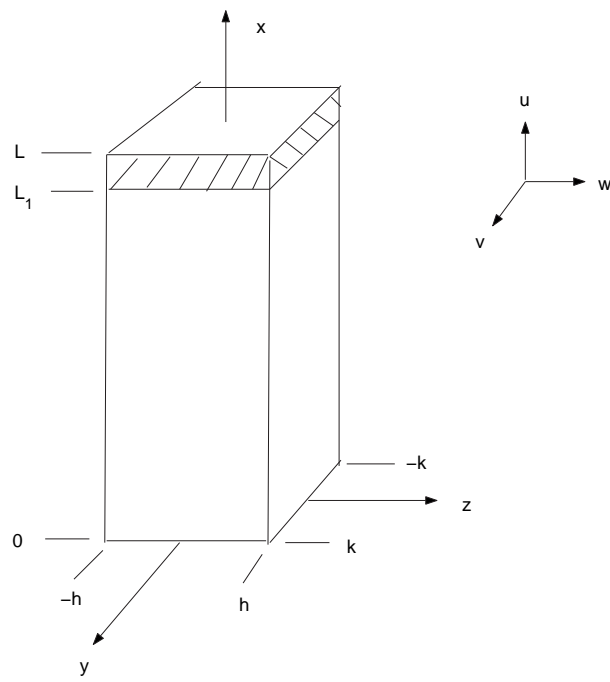


Figure 2: Formulation of the Tip Mass Model

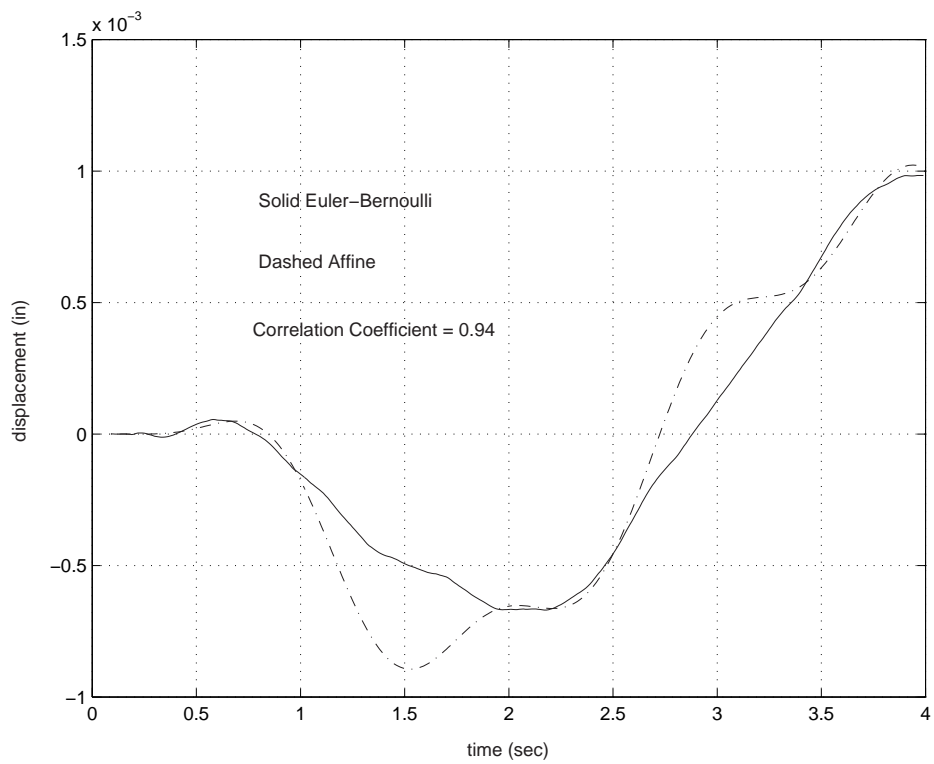


Figure 3: Comparison of tip displacements using the narrow plate and Euler-Bernoulli tip mass models

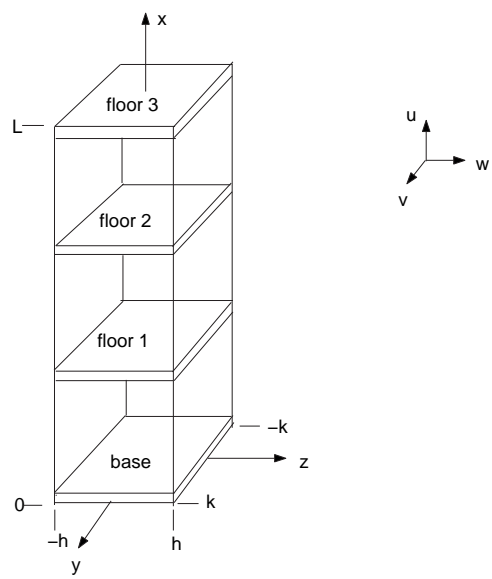


Figure 4: Basic structure for laboratory data

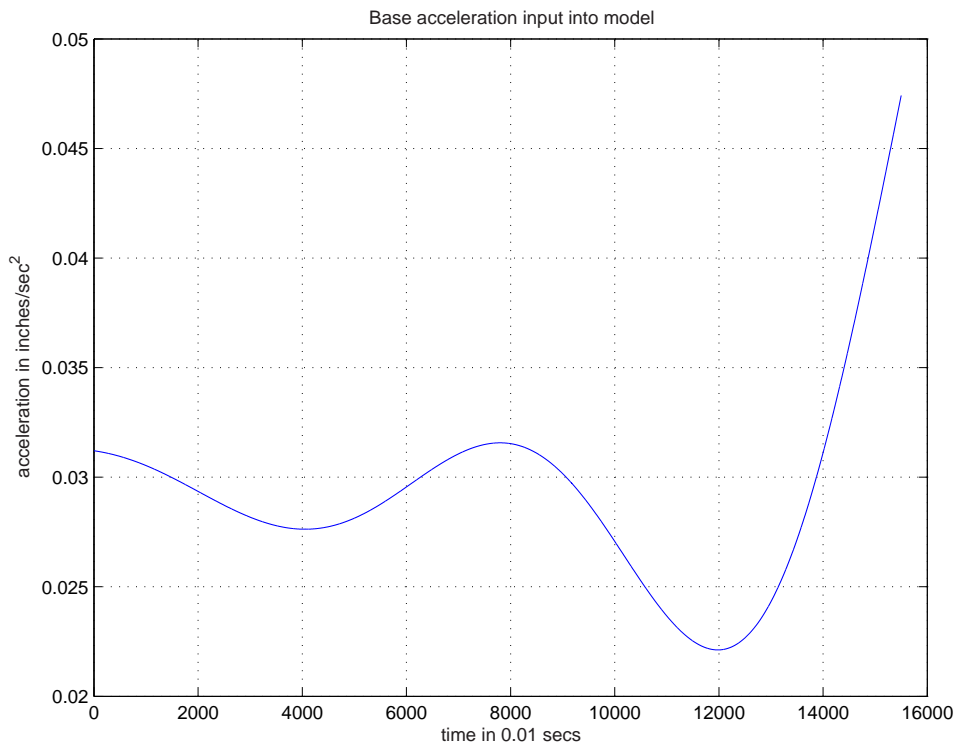


Figure 5: Wavelet approximation of the base acceleration

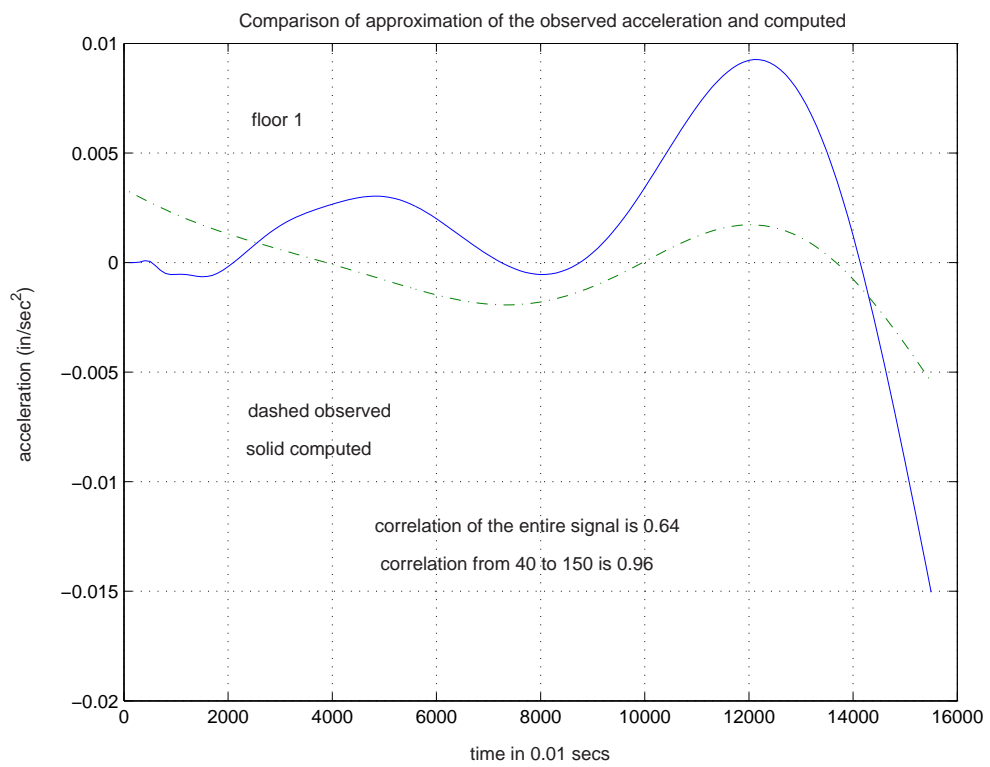


Figure 6: Wavelet approximation of the 1st floor acceleration and the model-computed acceleration

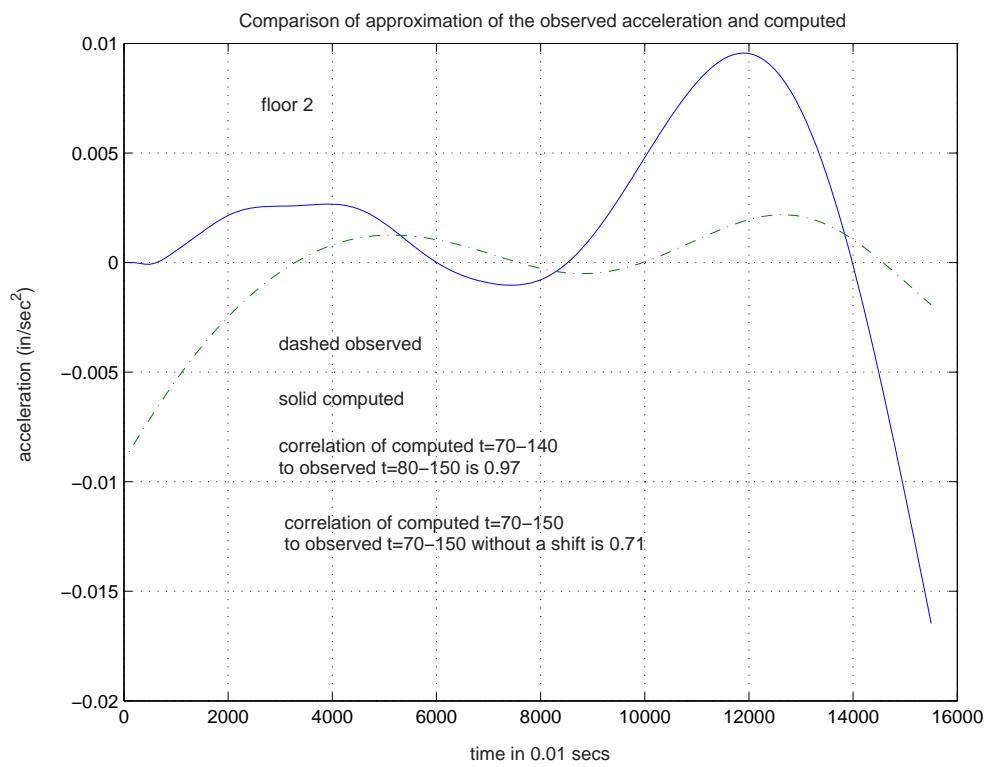


Figure 7: Wavelet approximation of the 2nd floor acceleration and the model-computed acceleration

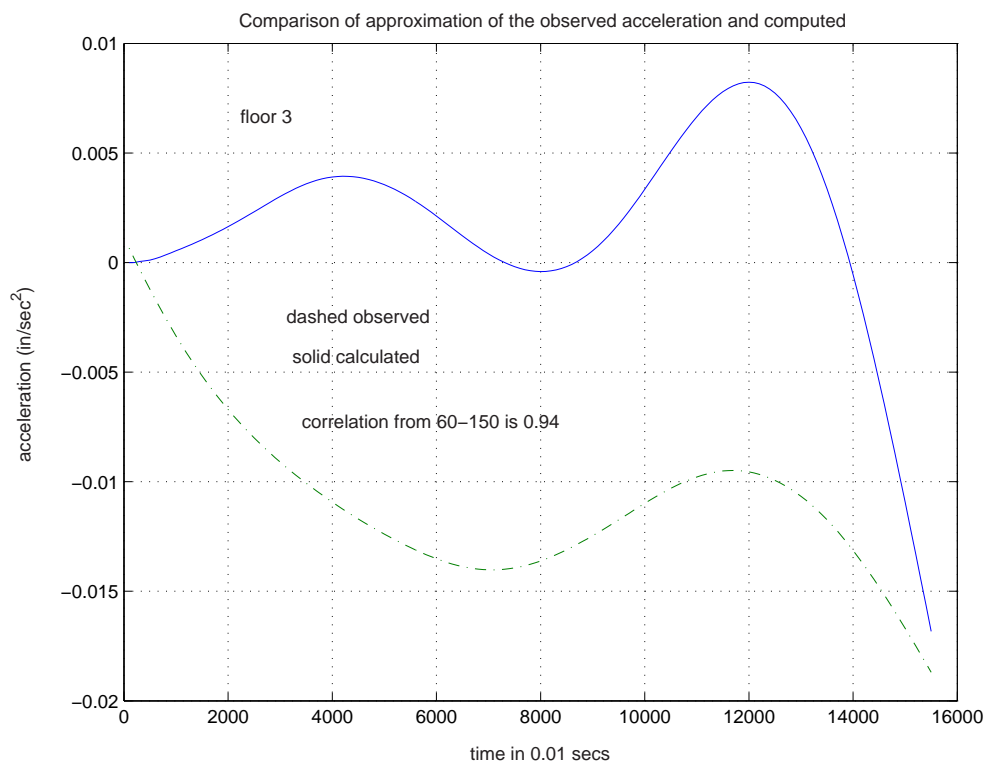


Figure 8: Wavelet approximation of the 3rd floor acceleration and the model-computed acceleration

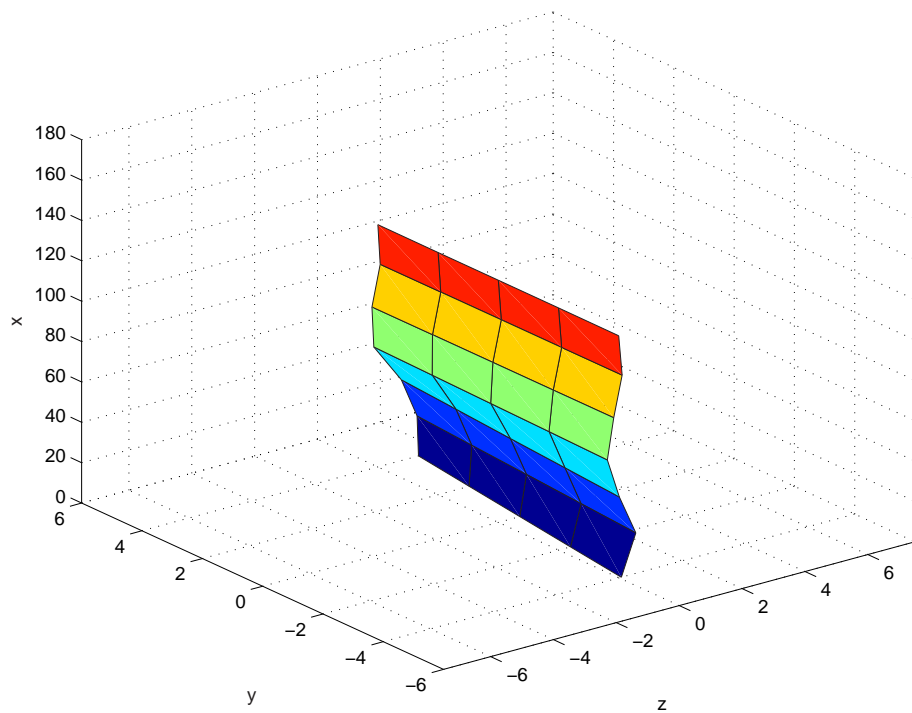


Figure 9: Deformation of the structure based on the model

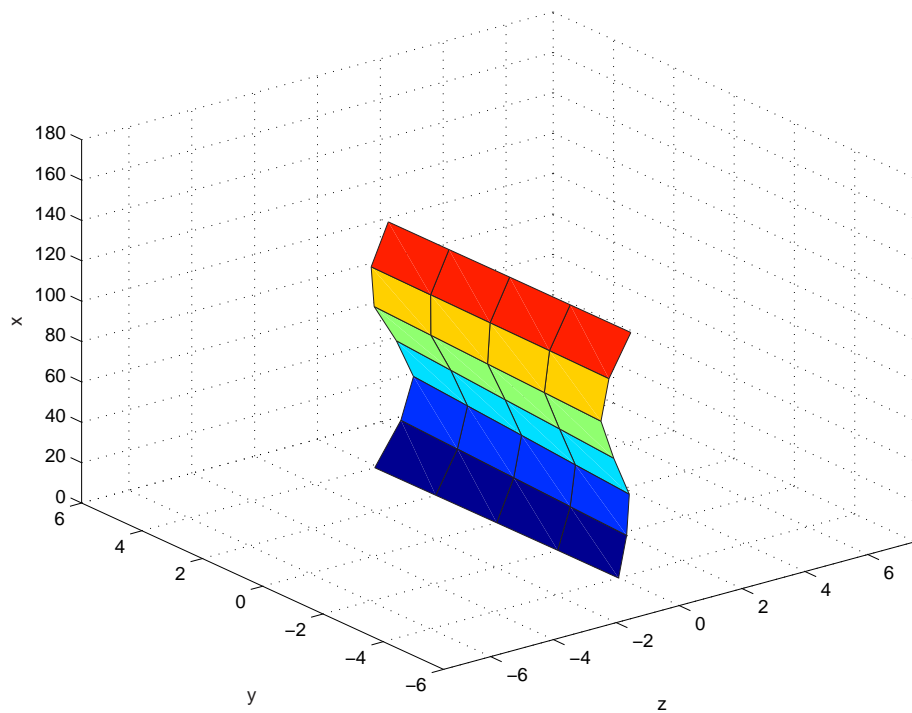


Figure 10: Deformation of the structure based on the model

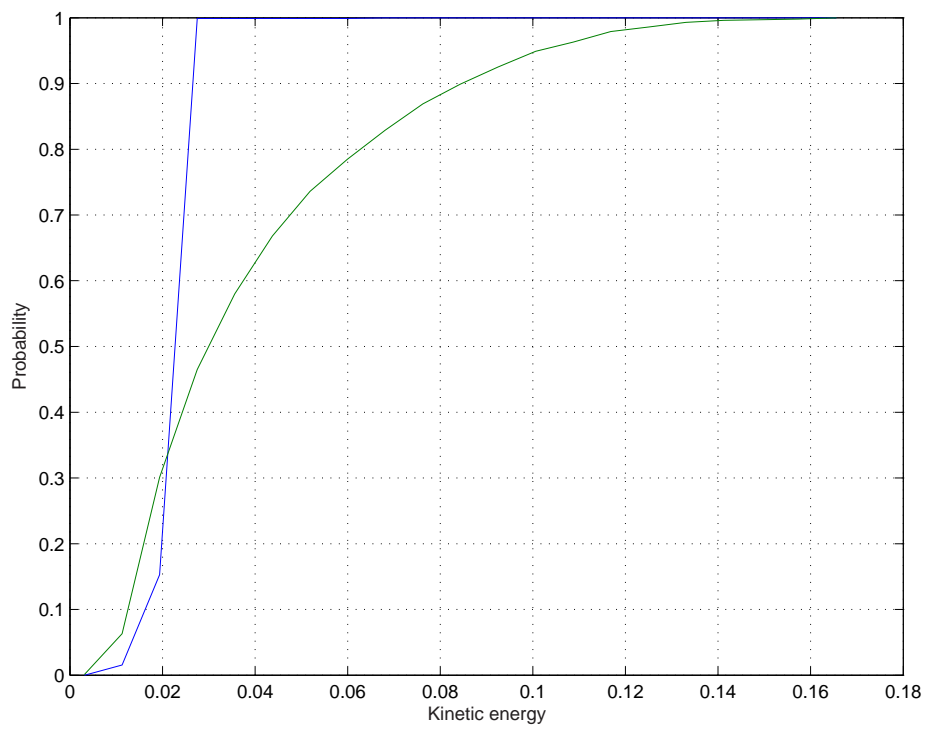


Figure 11: Cumulative distribution of the kinetic energy at mass 3